ACS APPLIED MATERIALS & INTERFACES

www.acsami.org
Research Article

Engineering Hyperechogenic Colloids with Clot-Targeting Capabilities from Platelet-Derived Membranes

Mark Louis P. Vidallon,*,¶ Mitchell J. Moon,¶ Haikun Liu, Yuyang Song, Simon Crawford, Boon Mian Teo, James D. McFadyen, Alexis I. Bishop, Rico F. Tabor, Karlheinz Peter,¶ and Xiaowei Wang*,¶

Cite This: ACS Appl. Mater. Interfaces 2024, 16, 55142−55154

Read Online

ACCESS | Metrics & More | Article Recommendations | Supporting Information

ABSTRACT: Thrombosis-related cardiovascular diseases remain the leading global cause of mortality and morbidity. In this study, we present a pioneering approach in the field of nanobiotechnology, with a focus on clinical translation, aimed at advancing early diagnosis and enhancing treatment options for thrombotic disorders. We introduce the fabrication of Platelet Membrane-Derived Bubbles (PMBs), which exhibit distinctive characteristics compared to conventional nanoparticles. These PMBs possess an average diameter of 700 nm and a negative ζ-potential, mirroring the attributes of parent platelet membranes. Utilizing diagnostic ultrasound imaging, we demonstrated the ability to visualize PMBs as hyperechogenic entities in agarose phantoms *in vitro* and in live mice *in vivo*. Furthermore, through confocal laser microscopy, we verified the retention of crucial transmembrane proteins, such as CD41 (GPIIb) and CD42 (GPIb), pivotal in conferring platelet-specific targeting functions. Importantly, our platelet aggregation studies confirmed that PMBs do not induce platelet aggregation but instead adhere to preformed platelet-rich *in vitro* thrombi. Overall, our work showcases the safe and precise utilization of PMBs to directly target acute thrombosis induced by laser injury in murine mesenteric veins *in vivo*, as visualized through intravital microscopy. In conclusion, we have successfully developed a rapid method for generating PMBs with unique ultrasound-directed and thrombus-targeting properties. These exceptional attributes of PMBs hold significant promise for advancing the field of ultrasound diagnostic thrombus imaging and clot-targeted therapy in the clinical context.

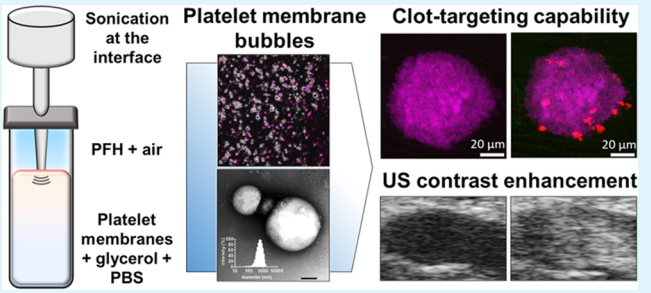

KEYWORDS: *bubbles, cell membrane, platelet, thrombus targeting, ultrasound contrast agent*

1. INTRODUCTION

Cardiovascular diseases, particularly thrombosis, remain the leading causes of mortality and morbidity worldwide. Thrombi are formed by crossbridging interactions between platelets and fibrin(ogen), which can result in vascular occlusion leading to tissue ischemia with potentially life-threatening consequences. Invasive interventional techniques, such as percutaneous coronary interventions or thrombectomy (manual clot retrieval), are the gold standard treatment for restoring blood flow, while fibrinolytic drugs are typically used to dissolve thrombi when interventional techniques are not feasible or available.[1] However, pharmacological thrombolysis is associated with a limited success rate (∼50%) and a high risk of potentially deadly bleeding complications. In addition to challenges in regard to effectivity and adverse effects in relation to thrombosis treatments, current diagnostic detection techniques for thrombi, such as ultrasound and computed tomography (CT), have inherent limitations as they rely on identifying the absence of a signal indicating reduced or occluded blood flow and, hence, may not be sensitive enough for small or microthrombi such as those seen in small arteries in cardiac ischemia reperfusion injury.[2−4] Therefore, imaging strategies that target epitopes which are thrombus-specific, such as those present on activated platelets and fibrin, are highly sought after for direct visualization of thrombi in patients.

To overcome the limitations associated with pharmacological thrombolysis,[5] several strategies have been employed: direct functionalization of drug molecules with targeting moieties; genetic engineering to create antibody−drug fusion constructs for active drug delivery; and development of nanobiotechnology for dual diagnostic and therapeutic approaches.[6,7] Colloidal materials, encompassing micro- and nanoparticles, emulsion nanodroplets, and microbubbles,

Received: July 19, 2024
Revised: September 25, 2024
Accepted: September 25, 2024
Published: October 3, 2024

present themselves as versatile candidates for targeting and therapeutic applications in thrombosis and beyond.

A groundbreaking approach to enhancing colloidal materials involves biointerfacing, utilizing cell membranes to imbue colloids with surface functionalities akin to native cells. Diverse cell-derived membranes have been employed, facilitating applications across various nanoparticle systems (such as metal/metal oxides and polymeric nanomaterials), emulsions, microbubbles, and bioactive molecules. Because of the diversity of cell membranes, in combination with possible payloads, biointerfaced colloids boast a wide range of applications, ranging from immune suppression and targeted drug delivery to toxin removal, sensing, diagnostics, and theranostics.[8−13] The multitude of cell membrane options also offer versatility in functionalization and targeted applications across various disease areas.

In a recent advance, our research team successfully developed a bubble system incorporating red blood cell membranes with enhanced ultrasound properties.[14] In order to extend our capability to target thrombosis, we are motivated to expand our repertoire to encompass other types of blood cell membranes. Platelet membranes present an ideal biointerfacing component for targeting cardiovascular diseases given their innate capability to interact with activated platelets, activated vascular endothelium, foam cells, and collagen.[15] These interactions are achieved through the adhesive proteins expressed on the platelet surface, such as GPIIb/IIIa (the major ligand for fibrin(ogen) and platelet−platelet interactions),[16] GPIb (the main ligand for von Willebrand factor [vWF] and collagen),[17] and GPVI (the major ligand for collagen),[18] which allow platelets to bind to thrombi, activated endothelium, and "injured" vascular walls. While there have been reports on thrombus-targeting capabilities of platelet membrane−functionalized materials in the literature,[19] most of these systems are either supersmall nanobubbles or nanocolloids, which in comparison to microbubbles are generally unstable (Laplace pressure bubble catastrophe) and poorly echogenic (higher resonance frequency with smaller diameter),[20−22] limiting their utility as contrast agents for fundamental ultrasound imaging.[23]

Ultrasound imaging has emerged as a compelling choice in medical research and clinical practice alike due to its cost-effectiveness, noninvasiveness, relatively high resolution, real-time capabilities, and portability compared to more complex imaging modalities like CT and magnetic resonance imaging (MRI).[24,25] To leverage these advantages further, acoustically active, lipid-shelled bubbles that offer ultrasound tracking capabilities have been developed. This innovative combination has opened up exciting possibilities, mainly for cancer detection and treatment and with emerging utility in cardiovascular diseases, where it finds diverse applications and holds promising potential for advancing medical diagnostics and treatments.[8,26] Notable applications include: Nox2 siRNA-loaded lipid nanobubbles with platelet membrane coating for atherosclerosis treatment utilizing the natural ability of platelets to bind to atherosclerotic plaques, mixed with targeted ultrasound-induced cavitation;[27] acoustically active platelet membrane−liposome bubbles for detection of damaged endothelium in sepsis-induced kidney injury;[28] and platelet membrane nanobubbles, which target acute ischemic stroke lesions.[29]

Here, we report the fabrication of platelet membrane−interfaced microbubbles (PMBs) as a dual functionality colloidal material, functioning as both an ultrasound contrast agent and a thrombus-targeting colloid. The functionalities of the platelet membrane surface proteins confer the targeting function, while the gas load confers strong ultrasound backscattering properties. This work also features a quick and gentle fabrication method allowing production of platelet membrane−interfaced bubbles at meso- to microscales which result in strong ultrasound contrast enhancement at relatively low concentrations.

2. RESULTS AND DISCUSSION

2.1. Fabrication and Structural Characterization of PMBs. Human platelets were isolated from whole blood through differential centrifugation (see Section 4.2 in the Experimental Section). Platelets were then subjected to three freeze−thaw cycles with centrifugation and redispersion in fresh buffer solution to free and wash away the intercellular contents and obtain empty platelet membranes. This step ensured that the membranes did not undergo irreversible morphological changes due to activation, which may result in the loss of the desired spheroidal morphology of the membranes and alteration of the membrane components, structures, and functions that are important in clot-targeting.

PMBs were fabricated utilizing sonication with optimized parameters according to our prior publication[14] and patented process.[30] Sonication at the gas−liquid interface serves two roles in this method: (1) dispersing the gas molecules from the headspace into the liquid phase; and (2) inducing acoustic cavitation of dispersed gas bubbles, triggering various physical effects that partially disrupt the platelet cell membranes. This method allows gas bubbles to be entrapped within the platelet membranes, followed by spontaneous resealing of the membranes. Entrapment of the gas is ensured by utilizing glycerol as a viscous continuous medium and a perfluorohexane (PFH)−air mixture as the headspace component based on previously optimized parameters.[14] Highly viscous glycerol prevents coalescence of the dispersed gas molecules, allowing these molecules sufficient time to be captured and stabilized within the lipid shell. PFH is an ideal gas load since perfluorocarbon (PFC) gases have lower water solubility than air, which effectively delays gas diffusion.[31,32] Furthermore, PFH molecules are expected to have a strong affinity for the hydrophobic tails of platelet membrane phospholipids[33] and are reported to intercalate between the hydrophobic tail groups of phospholipid molecules.[34]

Dynamic light scattering (DLS) size distribution plots in Figure 1A,B show that ultrasonication changed the initial narrow size distribution of platelet membranes in the micrometer regime (mean diameter = 2 μm) to smaller colloidal materials (PMBs) with a wide size range of 50 nm to 1.7 μm and a mean diameter of 700 nm. The observed change in size distribution is associated with an unchanged ζ-potential of the platelet membranes (−14 mV), indicating that the resulting PMBs retain the negative surface charge of the parent platelet membranes and are colloidally stable in dispersion. Plots showing the changes in the mean diameter, polydispersity, ζ-potential, and size distribution of platelet membranes at different stages of the fabrication process are shown in Figure S1 in the Supporting Information. The size distribution data from DLS is supported by transmission electron microscopy (TEM) and optical microscopy imaging (Figure S2 in the Supporting Information). Characterizing PMBs presents several challenges due to their inherent buoyancy, which

https://doi.org/10.1021/acsami.4c12024
ACS Appl. Mater. Interfaces 2024, 16, 55142−55154

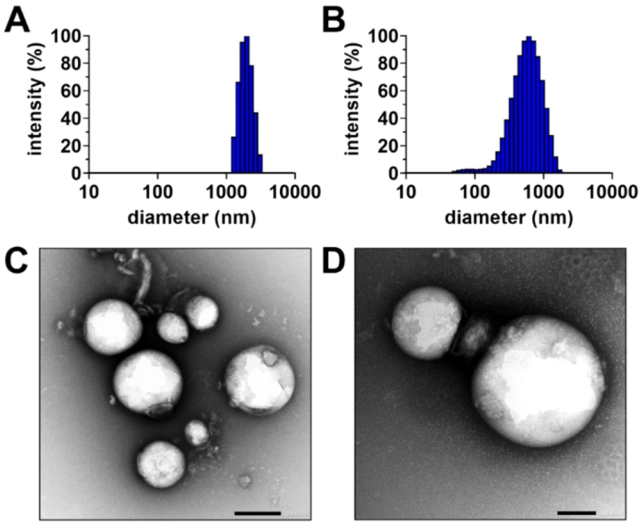

Figure 1. Structural characterization of PMBs. Dynamic light scattering size distribution plots of: (A) platelet membranes after three freeze−thaw cycles; and (B) PMBs produced via sonication. (C and D) Representative transmission electron microscopy images showing the structure of uranyl acetate−stained PMBs. Scale bars = (C) 200 nm and (D) 100 nm.

causes uneven distribution and varying focal planes, making consistent imaging and size measurements difficult. TEM was used to examine the structure of PMBs which revealed PMBs as spherical structures with high contrast regions representing platelet membrane "shells" around a low-electron density core, corresponding to the encapsulated gas (Figure 1C,D). This method favors smaller particles and struggles with larger ones, thus not fully representing the size distribution of PMBs. To mitigate these issues, confocal microscopy was employed on settled, unfixed PMBs to corroborate the DLS and TEM size data, however, buoyancy still led to out-of-focus particles. A brightfield binary contrast mask helped to accentuate in-focus particles and exclude many out-of-focus particles prior to size measurements, with results aligning with DLS measurements (Figure S2 in the Supporting Information). Notably, DLS offers a comprehensive portrayal of PMB size distribution, capturing both smaller structures emphasized by TEM and larger ones observed in optical microscopy, addressing resolution and focusing challenges on imaging techniques.

2.2. Biological Properties of Platelet Membrane−Interfaced Bubbles. *2.2.1. Platelet Receptor Expression and Biological Properties of PMBs.* Prior to testing the acoustic response of the produced PMBs, the unique surface functionalities of these materials were first explored. Confocal microscopy revealed that the PMBs were spherical structures which exhibited a large refractive index difference from the surrounding aqueous medium producing a "lens" effect typical of gas-filled bubbles (Figure 2A). During imaging, the PMBs retained their spherical structures, unlike washed human platelets that spread across the glass substrate (Figure 2B). Fluorescent labeling of the PMBs revealed that they retained two of the key platelet adhesion receptors: CD41 (the GPIIb subunit of GPIIb/IIIa), which is required for platelet−platelet interaction through its binding of fibrin(ogen) (Figure 2A, top row), and CD42b (the GPIb subunit of the GPIb−IX−V complex), which primarily binds vWF (Figure 2A, middle row). Notably, GPVI was not detected on the PMBs using immunofluorescence microscopy (Figure 2A, bottom row), most likely because GPVI was shed during freeze−thawing. GPVI shedding is a natural process contributing to platelet function in thrombosis and hemostasis, although with its precise regulation and functional consequence not yet fully understood.[35] The shedding of GPVI from the platelet membrane is known to occur upon platelet activation,[36] but notably has also been observed following cryopreservation and cold storage of human platelets, without necessarily being associated with platelet activation.[37,38] Expression of CD41, CD42b, and GPVI was confirmed on human washed platelets by immunofluorescence microscopy (Figure 2B). Receptor expression was also investigated by flow cytometry (Figure 2C−F). As expected, PMBs were smaller and less granular (low forward scatter and low side scatter, respectively) compared to human washed platelets (Figure 2C,D). In line with the confocal microscopy results, we were able to confirm the expression of CD41, and CD42b, and a clear reduction of GPVI expression (Figure 2C), whereas all three receptors were detected at high expression levels on platelets (Figure 2D). Furthermore, we also confirmed that CD61 (the GPIIIa subunit of GPIIb/IIIa) is expressed on both PMBs and platelets (Figure 2C,D). These findings are consistent with our aim to use PMBs as tools for targeting thrombi. The central receptor for binding/localizing to thrombi is primarily GPIIb/IIIa and secondarily the GPIb−IX−V complex at high shear stress, whereas GPVI is dispensable as PMBs are designed to target thrombi directly and are not dependent on collagen binding. As PMBs are heterogeneous in size (Figure 1B), we have carefully gated the majority of our particles to ensure that the measurements were representative and accurate. This is because their heterogeneity could potentially confound flow cytometry gating. In addition, we also performed flow cytometry on isolated platelet membranes (PLT M), which are the shells of PMBs prior to gas loading. We confirmed that PLT M exhibits the same platelet expression profile as PMBs, expressing CD41/CD61 and CD42b but not GPVI (Figure S3 in the Supporting Information).

As PMBs are derived from human platelets, it was important to assess if they can become activated by agonist stimulation, and how they interact with platelets in solution. To achieve this, we first performed flow cytometry to examine the activation status of unstimulated and stimulated PMBs and human platelets. Both were incubated with fluorescence-labeled antibodies against CD62P (P-selectin is mobilized to the platelet surface from platelet α granules upon activation) and the active conformation of GPIIb/IIIa (detected by the antibody PAC-1). In PMBs neither of these activation markers were detected in unstimulated or stimulated (thrombin 1 U mL^{-1}) conditions (Figure 2E). In contrast, there was a clear positive signal detected for both activation markers in stimulated compared to unstimulated platelets (Figure 2F). We next performed light transmission aggregometry (LTA) in human platelet-rich plasma (PRP) to verify whether PMBs promoted and/or contributed to platelet aggregation. PMBs, platelet membranes, or vehicle (PBS−glycerol) were added to human PRP prior to agonist stimulation. As shown in Figure 2G (region highlighted in blue), upon addition of the samples to PRP no decrease in optical density (platelet aggregation) was observed, indicating that the PMBs, PLT M, or vehicle (PBS−glycerol) did not cause platelet aggregation. It can be noted that upon addition of PMBs, there was an increase in optical density, which followed a similar trend over time to the other samples. This can be attributed to the refractive index

https://doi.org/10.1021/acsami.4c12024
ACS Appl. Mater. Interfaces 2024, 16, 55142−55154

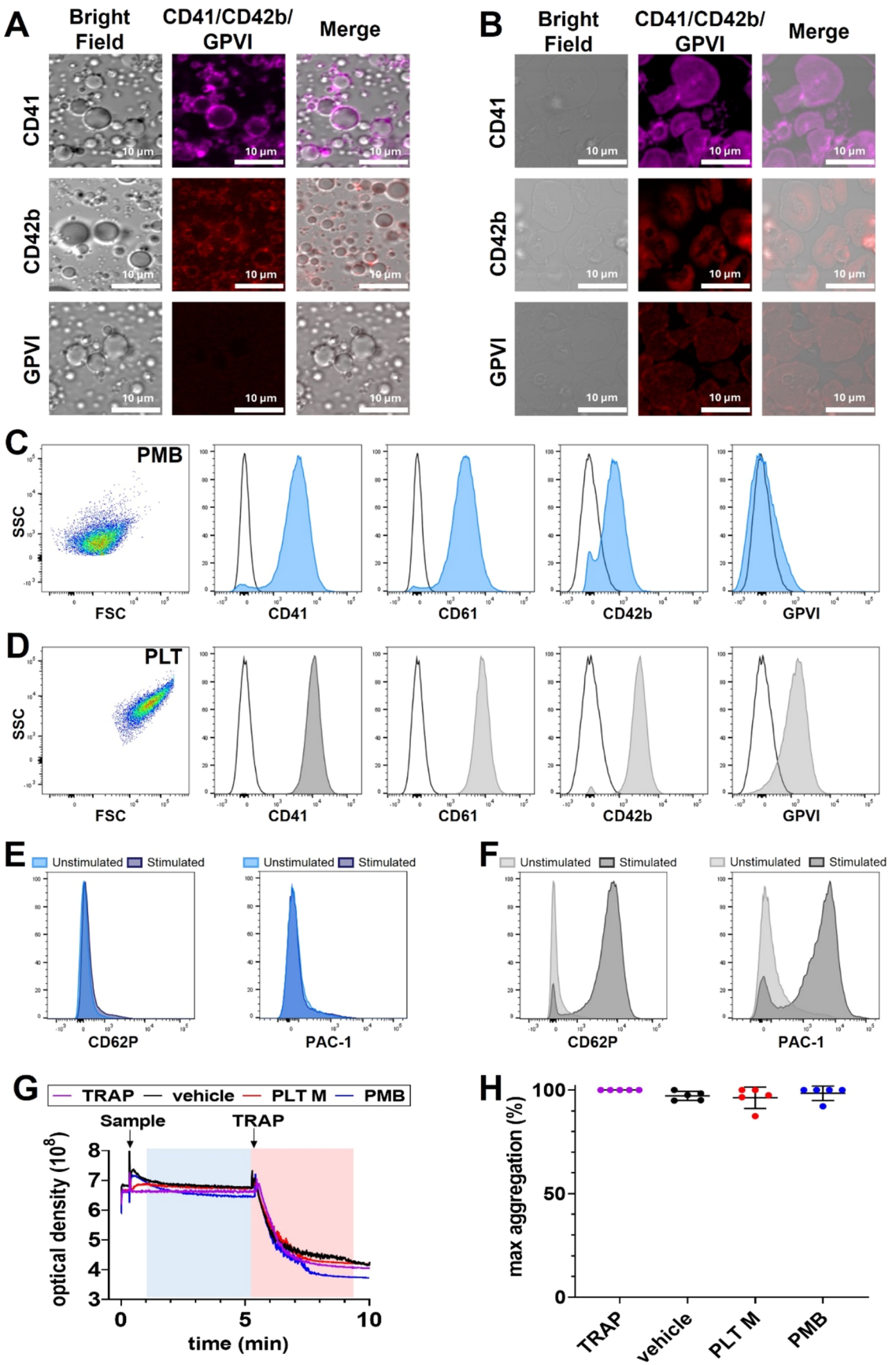

Figure 2. Platelet receptor expression and biological properties of PMBs. (A) Confocal photomicrographs showing expression of CD41, CD42b, and GPVI on PMBs. Scale bar = 10 μm. (B) Confocal photomicrographs showing expression of CD41, CD42b, and GPVI on human washed platelets. Scale bar = 10 μm. (C) Flow cytometry data of PMBs showing forward vs side scatter (FSC vs SSC) dot plots and histograms of CD41, CD61, CD42b, and GPVI expression on PMBs (blue) compared to isotype control antibodies (fluorescently labeled mouse IgG; black). (D) Flow

https://doi.org/10.1021/acsami.4c12024
ACS Appl. Mater. Interfaces 2024, 16, 55142−55154

Figure 2. continued

cytometry data of human washed platelets (PLTs) showing forward vs side scatter (FSC vs SSC) dot plots and histograms of CD41, CD61, CD42b, and GPVI expression on platelets (gray) compared to isotype control antibodies (fluorescently labeled mouse IgG; black). (E) Flow cytometry histograms showing unstimulated vs stimulated (thrombin 1 U mL^{-1}) PMBs. PMBs were labeled with an antibody against CD62P (P-selectin; left) or the antibody PAC-1 against activated GPIIb/IIIa (right). (F) Flow cytometry histograms showing unstimulated vs stimulated (thrombin 1 U mL^{-1}) human washed platelets. Platelets were labeled with an antibody against CD62P (P-selectin; left) or the antibody PAC-1 against activated GPIIb/IIIa (right). (G) Representative light transmission aggregometry curves. Platelet membrane bubbles (PMB), platelet membranes (PLT M), or vehicle (PBS−glycerol) were added to human PRP and no aggregation was recorded (highlighted in blue). After 5 min platelets were stimulated with TRAP (30 μM) and platelet aggregation was recorded. Platelet aggregation was not impacted (highlighted in red). (H) Quantification of maximum platelet aggregometry compared to untreated PRP stimulated with TRAP (30 μM). Data presented as Mean ± SD (n = 5).

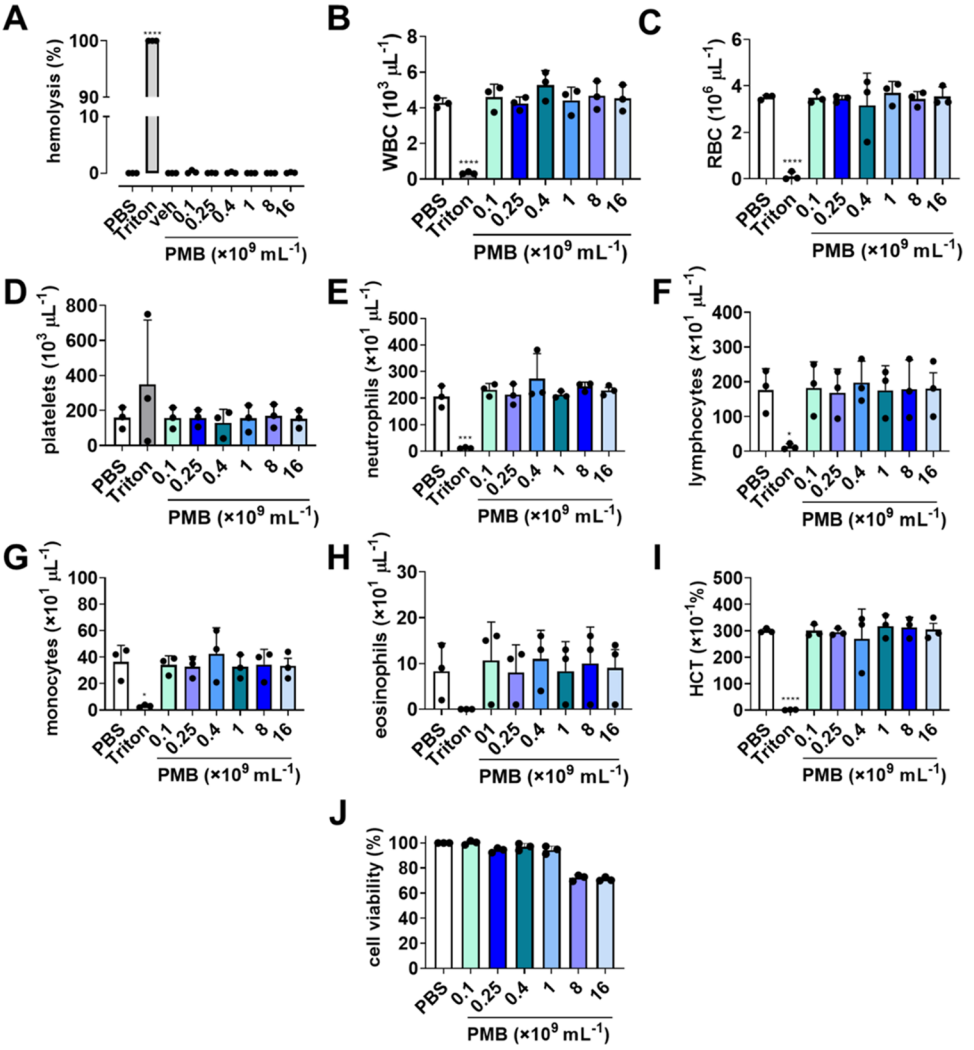

Figure 3. *In vitro* biocompatibility of PMBs. (A) Hemolysis in human whole blood, induced by Triton X-100, PBS, vehicle (PBS containing glycerol), and varying concentrations of PMBs (final concentrations of 0.1−16 × 10^9 PMB mL^{-1}). Data presented as Mean ± SD normalized to Triton X-100 (100% hemolysis) (n = 3). Cell counts of (B) white blood cells, (C) red blood cells, (D) platelets, (E) neutrophils, (F) lymphocytes, (G) monocytes, and (H) eosinophils and (I) hematocrit obtained using an automated cell counter after treatment with PBS, Triton X-100, or varying concentrations of PMBs (final concentration 0.1−16 × 10^9 PMB mL^{-1}). Data presented as Mean ± SD (n = 3). **** $p < 0.0001$, one-way analysis of variance (ANOVA) with multiple comparisons vs PBS. (J) MTT cell viability of human fibroblasts treated with PBS and varying concentrations of PMBs (final concentrations of 0.1−16 × 10^9 PMB mL^{-1}).

difference between the PRP and the PMBs, which were in a turbid dispersion (Figure S4 in the Supporting Information). This was confirmed through the addition of PMBs to platelet-poor plasma (PPP), whereby the same increase in optical density was observed in the absence of platelets (Figure S5 in the Supporting Information). After 5 min, all of the samples were treated with thrombin receptor-activating peptide (TRAP) to stimulate platelets and thereby induce platelet aggregation (Figure 2G, region highlighted in red). Following TRAP treatment, all samples showed reduced optical densities, denoting platelet aggregation, with no difference in their final optical density and therefore no inhibition of platelet aggregation at the end point (Figure 2H). Taken together, the flow cytometry and LTA data suggests that PMBs neither

https://doi.org/10.1021/acsami.4c12024
ACS Appl. Mater. Interfaces 2024, 16, 55142−55154

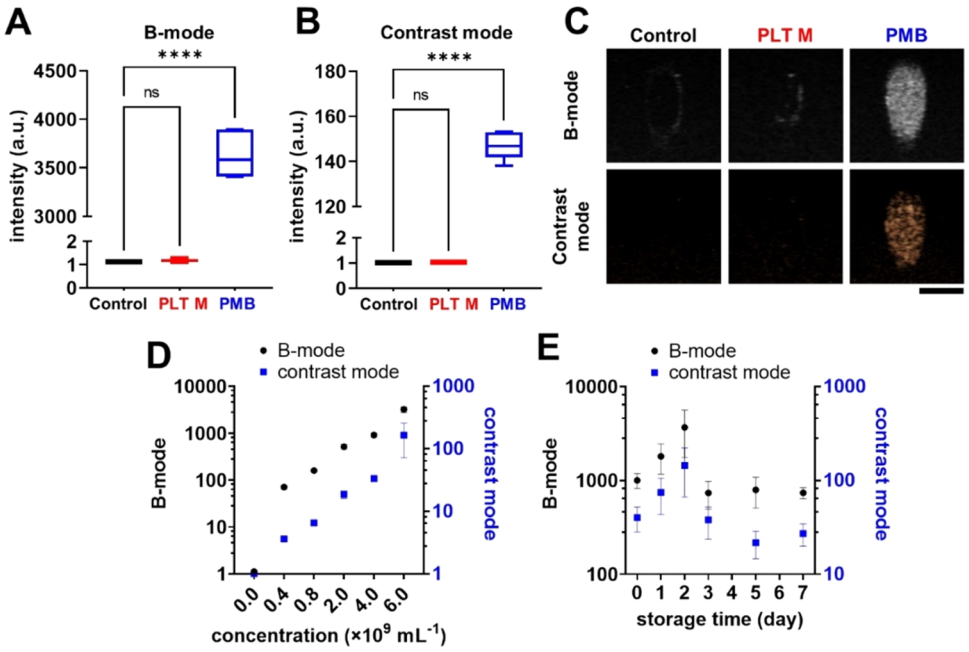

Figure 4. *In vitro* ultrasound imaging with PMBs. Ultrasound contrast enhancement based on: (A) B-mode and (B) contrast-mode ultrasonograms of tissue-mimicking phantoms with control (PBS), platelet membranes (PLT M), and PMBs (4.0×10^8 bubbles mL^{-1}), relative to PBS. Each data point represents Mean ± SD ($n = 3$); **** $p < 0.0001$ by one-way ANOVA. (C) Representative ultrasonograms with control, PLT M, and PMB. Scale bar = 2 mm. Ultrasound contrast enhancement in B-mode and contrast-mode imaging of tissue-mimicking phantoms with (D) different concentrations of PMB; and (E) with 4.0×10^8 bubbles mL^{-1} at different time points during a one-week storage stability study in concentrated form at 4 °C.

respond to stimulation by platelet agonists, nor do they induce, impair, or enhance platelet aggregation, and, hence, are expected to be safe in regard to platelet interactions.

2.2.2. In Vitro Biocompatibility. As a potential *in vivo* imaging and drug-delivery platform, the effect of PMBs on human whole blood was assessed *in vitro* using a hemocompatibility assay. Increasing concentrations of PMBs were combined with human whole blood for 1 h, the plasma was collected, and hemolysis was measured using 550 nm absorbance compared to the positive control (Triton X-100). No hemolysis was observed in blood combined with PMBs at all tested concentrations, $0.25-16 \times 10^9$ PMB mL^{-1} (Figure 3A). Complete blood counts (Figure 3B–I) were also performed on whole blood incubated with PMBs using an automated cell counter (Sysmex). No differences were observed between vehicle (PBS)- or PMB-treated samples. Moreover, to demonstrate compatibility with human cells, we conducted MTT cell viability assays with human fibroblasts using varying concentrations of PMBs. The results in Figure 3J revealed no significant alteration in cell viability within the range of $0.1-1.0 \times 10^9$ bubbles per mL treatment. However, at intentionally elevated, suprapharmacological doses, reduction in cell viability was observed. It is crucial to emphasize that, in a therapeutic context, upon injection into the bloodstream, PMBs undergo immediate dilution, leading to lower systemic concentrations. Furthermore, it is worth noting that this *in vitro* model does not account for immediate clearance, implementing an extended 24-h static incubation and exposure period of the cells to the sample, portraying a more extreme scenario in an *in vivo* experimental setup. From these results and those from the platelet aggregation data, it can be concluded that PMBs are biocompatible and suitable for targeting thrombi *in vivo*. This observation is in concordance with PFCs being used previously as artificial blood substitutes and oxygen-carrying agents for multimodal imaging and therapies.[39,40]

2.3. Visualization of PMBs Using Ultrasound Imaging *In Vitro* and *In Vivo*. Ultrasound imaging is a noninvasive and real-time diagnostic imaging technique with a broad application range and practical advantages including cost-effectiveness, easy accessibility, and portability. This imaging modality can be used alone for effective diagnostics and evaluating pathological progression and efficacy of clinical treatments, or to complement other structural and functional imaging techniques. Colloids, especially bubbles, can be introduced into the bloodstream to enhance ultrasonograms by providing superior visual contrast, particularly for organs with limited vascularization or in differentiating tissues that possess similar acoustic properties. Moreover, these colloidal materials can be effectively monitored using ultrasound, which serves as a tracking system with precise targeting capabilities. To assess the feasibility and efficacy of utilizing PMBs as contrast agents for ultrasound imaging, their ability to enhance contrast was evaluated through *in vitro* and *in vivo* testing.

2.3.1. In Vitro Model—Tissue-Mimicking Phantoms. To evaluate the ultrasound contrast enhancement by the PMBs, freshly prepared bubble dispersions were imaged in agarose phantoms that mimicked the acoustic properties or echogenicity of human tissues. Figure 4A–C demonstrate the strong ultrasound contrast enhancement in both brightness (B)-mode and contrast-mode by the PMBs, in comparison to platelet membranes and PBS (control). Figure 4D shows that the PMBs exhibited a concentration-dependent increase in ultrasound contrast (in mean gray values) with around 80- to 4000-fold and 2- to 200-fold increased contrast enhancement in B-mode and contrast-mode, respectively, for the concentration range of 4.0×10^8 to 6.0×10^{10} PMBs mL^{-1}. Ultrasound contrast enhancement by these materials can be attributed

https://doi.org/10.1021/acsami.4c12024
ACS Appl. Mater. Interfaces 2024, 16, 55142–55154

primarily to their strong backscattering property, arising from the large acoustic impedance mismatch between the surrounding PBS medium and the entrapped gas within the platelet membranes, as well as the resonance frequency of the bubbles potentially lying within the ultrasound transducer's operating frequency (19−25 MHz).

Short-term stability studies in static conditions (Figure S6A in the Supporting Information) revealed that visual contrast from the PMBs increased over the 1 h evaluation period. This observation is attributable to gravitational sedimentation of the bubbles due to the density of the entrapped glycerol within the membranes and partially due to possible coalescence of the bubbles which intensified the acoustic signal detected. To evaluate the long-term stability of PMBs, freshly fabricated bubbles were stored without dilution at 4 and 25 °C and then sampled for dilution and imaging at different time points. As shown in Figures 4E and S6B (in the Supporting Information), the contrast enhancement of PMBs which were stored at 4 °C and at 25 °C followed the same trends—a 10-fold increase in enhancement within the first 2 days, followed by a decrease in contrast enhancement from day 2. The former is attributable to the coalescence of smaller bubbles into larger bubbles, which intensified the acoustic signals detected. Large bubbles tend to lose their gas content eventually via diffusion and dissolution over time, as represented by the decrease in contrast enhancement from day 2. The most notable difference was the almost unchanged contrast enhancement of the sample stored at 4 °C from day 3 to day 7, in comparison with that of the sample at 25 °C. Overall, these observations indicate that a lower storage temperature prevents gas diffusion from the bubbles, thereby preserving the gas content and acoustic backscattering properties of PMBs. Taken together, these results also suggest that PMBs, like other ultrasound contrast agents, should ideally be used immediately upon fabrication or activation, but can be stored for a short period of time with reduced ultrasound enhancement in later use.

2.3.2. In Vivo Model—Ultrasound Imaging in Mice. To evaluate the ultrasound contrast enhancement by the PMBs in a biologically relevant system, PMB dispersions were injected into the femoral vein of mice and ultrasonograms of the inferior vena cava were acquired. As shown in Figure 5, approximately 1.8- and 2.5-fold increases in ultrasound contrast were observed in the ultrasonograms of mice inferior vena cava after a single bolus injection of 6×10^9 or 12×10^9 PMBs in PBS, respectively. This contrast enhancement is visually represented in Figure 5. Compared to the results of the ultrasonography in tissue-mimicking phantoms, the observed contrast enhancement *in vivo* was orders of magnitude lower, which is mainly attributable to the dilution of the PMBs in the bloodstream. Furthermore, there was minimal nonsample scattering in the simple tissue-mimicking phantoms while there was weakening of the incident ultrasound field *in vivo* due to biological scattering from multiple layers of tissues, organs, blood cells, etc. Despite these conditions, it is evident that PMBs retain their strong ultrasound backscattering properties. The results also indicate that PMBs are stable enough to endure the potentially destabilizing conditions in the vascular circulation, including temperature, high internal pressure, and complex blood components. Ultrasound contrast agents are widely used in clinical cardiology to enhance blood visibility within vessels and cardiac chambers, aiding in the assessment of blood flow during heart contractions. In preclinical cancer imaging, these agents accumulate in tumor areas,[41] while in

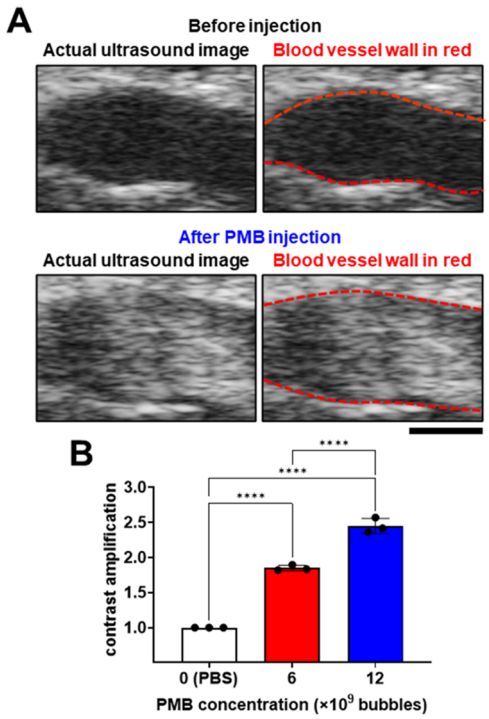

Figure 5. *In vivo* ultrasound imaging with PMBs. (A) Representative ultrasonograms of mouse inferior vena cava before and after a single bolus injection of PMBs. Scale bar = 1 mm. (B) Bar chart shows ultrasound contrast enhancement in ultrasonograms of mouse inferior vena cava upon multiple injections of 6×10^9 and 12×10^9 PMBs in PBS. Each data point represents Mean ± SD of 5 frames from 3 independent experiments (n = 3); **** $p < 0.0001$ by one-way ANOVA.

direct thrombosis imaging the targeted microbubbles bind to blood clots in the vessel lumen and are visualized as an increased contrast signal after the nonattached microbubbles' half-life has elapsed.[7,24] The increased brightness from these agents can lead to a less distinct vascular wall due to the initial brightness of the vessel wall compared to the lumen. Our PMBs demonstrated improved contrast intensity in the lumen, similar to commercially available and clinically used microbubbles, following a single bolus injection that created a pronounced wave of contrast through the vessel. Taken together, these observations strongly support the potential of PMBs as ultrasound contrast agents.

2.4. Targeting of Clots Using PMBs. *2.4.1. In Vitro Human Thrombosis Model.* Thrombus targeting was next assessed using an *in vitro* model of thrombosis. Platelet-rich thrombi were formed on a collagen surface using human blood and PMBs were allowed to adhere under blood flow. Fluorescence imaging revealed that the PMBs adhered predominantly to the thrombi, likely by interacting with exposed fibrin(ogen) on the thrombus surfaces (Figure 6A).[42] This hypothesis is supported by pretreatment of the PMBs with the GPIIb/IIIa inhibitor integrilin (eptifibatide, 50 μg mL^{-1}) prior to experimentation. In the presence of integrilin, PMB binding to thrombi was significantly lowered (Figure 6A−C), indicating that this interaction is largely GPIIb/IIIa-dependent. To control potential embolization of thrombi due to integrilin treatment, the thrombus area was measured, but was not significantly altered (Figure 6D).

https://doi.org/10.1021/acsami.4c12024
ACS Appl. Mater. Interfaces 2024, 16, 55142−55154

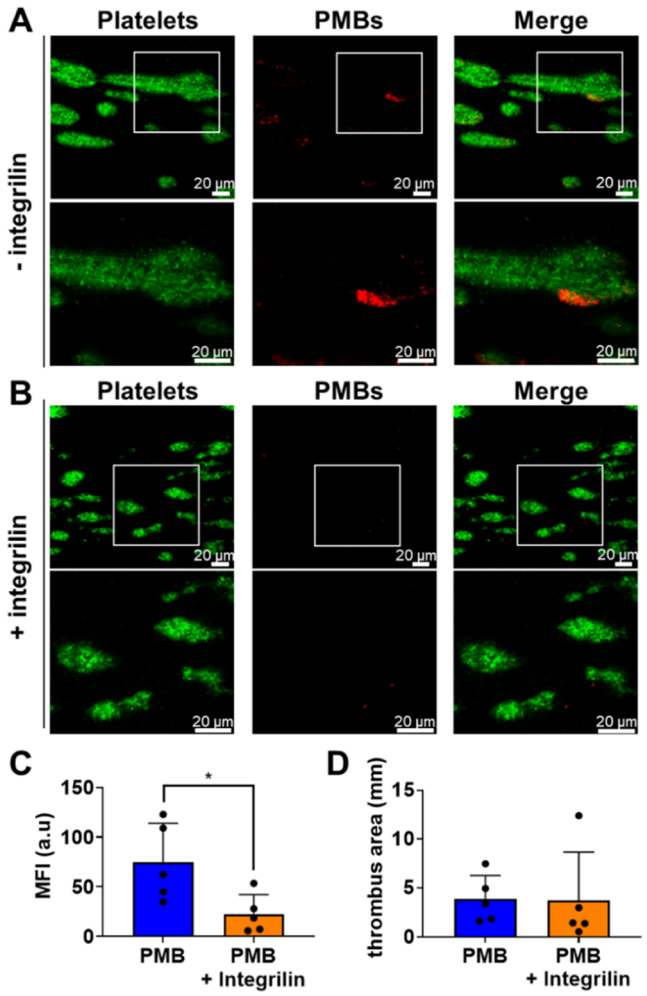

Figure 6. PMBs are biocompatible and can target human thrombi. Fluorescence confocal photomicrographs showing platelet-rich thrombi (green) and PMBs (red) in the absence (A) and presence (B) of the GPIIb/IIIa inhibitor integrilin (50 μg mL^{-1}). Images acquired at 60× (top) and 120× (bottom) magnification. White boxes denote magnified area. Scale bar = 20 μm. (C) Mean fluorescent intensity of thrombus-bound PMBs with and without integrilin treatment. Mean ± SD (n = average of 6 fields of view from 5 individual donors). * $p < 0.05$, unpaired t test with Welch's correction. (D) Thrombus area was not significantly altered by integrilin treatment. Mean ± SD (n = average of 6 fields of view from 5 individual donors). * $p < 0.05$, unpaired t test with Welch's correction.

These results corroborate the findings in Section 2.2, indicating that the preserved surface receptors on the platelet membranes at least partially retain their function as pristine platelets, enabling clot-targeting properties. Although PMBs were demonstrated not to interact with platelet aggregation in an LTA assay (Figure 2G), they were able to bind to thrombi in this *in vitro* model through GPIIb/IIIa. This can be attributed to the difference between soluble fibrinogen in platelet aggregometry (dependent on activated GPIIb/IIIa) and immobilized fibrinogen or fibrin on the thrombus surface (binding to active and importantly to nonactivated GPIIb/IIIa).[42] Furthermore, these observations clearly demonstrate, for the first time, the potential of PMBs as precision ultrasound diagnostic agents for blood clots, which can be further explored for *in vivo* imaging and potentially be employed in clot-targeting, ultrasound-based theranostic applications.

2.4.2. In Vivo Thrombosis Model. Having successfully shown that PMBs bind to human thrombi *in vitro*, we employed an intravital microscopy mouse model of *in vivo* thrombosis to show real-time binding of fluorescently labeled PMBs to a platelet-rich thrombus. Application of human platelet-derived materials were previously shown to be biocompatible and bind to mouse thrombi *in vivo*.[43] To directly visualize PMB binding to thrombi *in vivo*, a focused single-wavelength laser was used to induce endothelial damage in the mouse mesenteric vein. The subsequent thrombus was allowed to develop, stabilize, and consolidate (approximately 5 min) (Figure 7A,B, top rows). PMBs were administered intravenously and the thrombus was reimaged to assess PMB binding. Time series videos show that the PMBs circulated

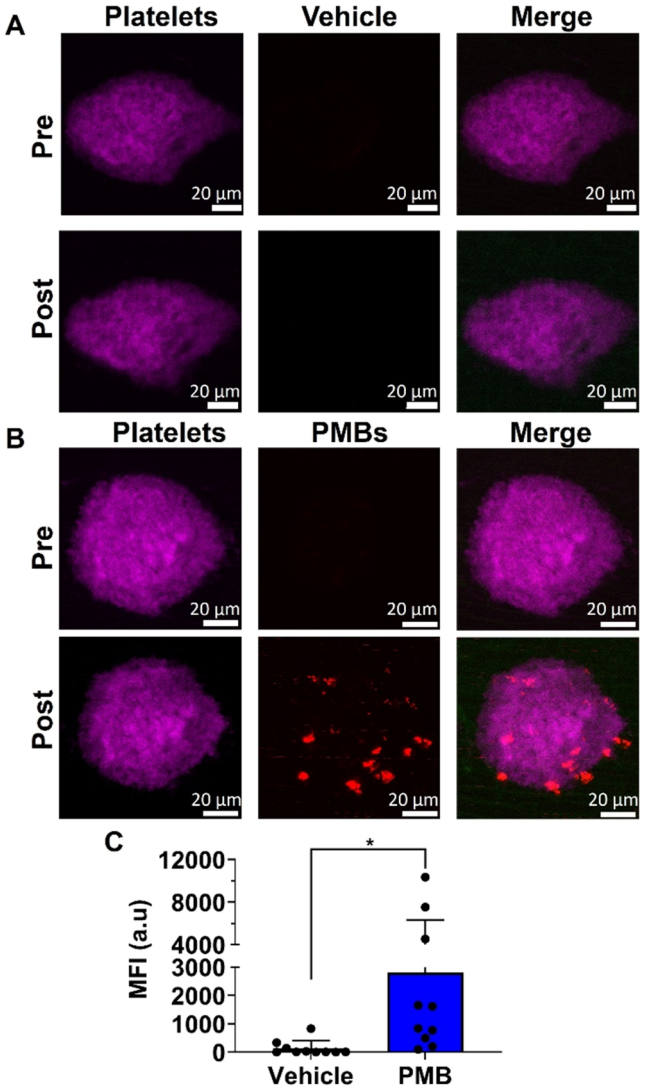

Figure 7. PMBs target mouse thrombi *in vivo*. Representative sum projections of thrombi formed in intravital laser-induced model of thrombosis before (top) and after (bottom) intravenous injection of 150 μL of (A) vehicle (PBS with $DiIC_{12}$) or (B) 12×10^9 $DiIC_{12}$–labeled PMBs in PBS solution. Visible are platelet GPIb (purple) and PMBs or free dye (red). Scale bars = 20 μm. (C) Mean fluorescent intensity in red channel (λ = 561 nm (excitation) and 597 nm (emission)) within area of thrombus from animals injected with vehicle or 12×10^9 PMBs in PBS solution. Mean ± SD (n = 10). * $p < 0.05$, unpaired t test with Welch's correction.

https://doi.org/10.1021/acsami.4c12024
ACS Appl. Mater. Interfaces 2024, 16, 55142−55154

through the vasculature and readily adhered to thrombi (Supplementary Video 1 in the Supporting Information). Analysis of *Z*-stacks taken of the thrombi showed increased fluorescence from $DiIC_{12}$-labeled PMBs compared to vehicle (PBS−glycerol containing $DiIC_{12}$) (Figure 7A−C). Similar to the findings using human thrombi *in vitro*, PMBs were observed only on the peripheries of the thrombus but did not incorporate into the stabilized, consolidated thrombus. To control for off-target labeling of the membrane dye ($DiIC_{12}$), mice were injected with a vehicle control (PBS−glycerol mixture) containing the same concentration of $DiIC_{12}$ used to label the PMBs (2 μg mL^{-1}). As $DiIC_{12}$ is not a platelet-specific membrane dye, some fluorescent events can be observed in circulation (Supplementary Video 2 in the Supporting Information); however, these cells did not adhere to the thrombus, indicating that the observed thrombus-bound particles were PMBs. When compared to the experimental results for the *in vitro* human thrombi binding (Section 2.4.1), the number of PMBs bound to the thrombus was modest, most likely due to the clearance of PMBs through the liver and lung (Figure S7 in the Supporting Information) and to species differences between human and mouse platelets. A key limitation of our study is the potential species cross-reactivity due to using PMBs derived from human platelet membranes in murine models. Although our preliminary findings show no adverse effects, this cross-species application could introduce immune responses that are not reflective of human clinical scenarios, complicating the interpretation of safety and efficacy data. Future studies should consider using humanized models or alternative approaches to better mimic the human immune environment and provide more clinically relevant safety assessments.

These findings confirm the advantages of PMBs as a novel tool for diagnostic imaging, which can be extended to theranostics. Thrombus-targeted nanoparticles have been studied as a mechanism for delivering targeted drug treatments such as thrombolytics[7,44] and cancer therapy.[45,46] Previous studies from our lab have explored the potential of commercially available microbubbles as thrombus-targeted contrast agents, and for targeted thrombolysis.[1,7,24] In these studies, various conjugation methods were employed to decorate the microbubbles with antibodies that specifically bind to activated platelets to facilitate thrombus targeting. Furthermore, many targeted nanoparticles often rely on indirect factors such as pH,[43] shear,[47] or external targeting factors such as magnetic targeting[48] or laser stimulation[44] to facilitate targeting and drug release. In comparison, PMBs offer the inherent ability to target thrombi, along with the advantage of being acoustically active for thrombosis diagnosis and monitoring, making them prime candidates for drug-loading and targeted drug delivery. Future work focusing on loading with fibrinolytic drugs, or conjugation of a fibrinolytic/antibody fusion construct onto PMBs are required to demonstrate their theranostic ability. This approach may achieve further benefits through controlled payload release via ultrasound bursting.[22]

3. CONCLUSIONS

We have engineered PMBs that are acoustically active colloids and demonstrate binding and thus targeting platelet-rich thrombi. PMBs were generated using a rapid fabrication method, being produced within a single day from the donor's whole blood or within minutes from stored platelet-derived membranes. The PMBs were found to be colloidally stable and morphologically distinct from human platelets. It is also noteworthy that the PMBs did not undergo structural transformation, unlike platelets that activate and spread on various interfaces. Most importantly in terms of physical properties, these materials have acoustic characteristics, owing to their gas content, making them ideal for ultrasound imaging-based tracking. In terms of bioactivity, the PMBs exhibited a significant level of binding to human thrombi *in vitro* in a whole-blood thrombosis assay. Importantly, our PMBs did not aggravate thrombosis and did not cause platelet aggregation. Furthermore, we demonstrated that the PMBs provided excellent binding to mouse thrombi *in vivo* in an acute thrombosis model using intravital microscopy. This was possible due to the retention of key platelet adhesion receptors and could be blocked using a GPIIb/IIIa inhibitor, indicating that thrombus binding of PMBs is GPIIb/IIIa-dependent. As PMBs are acoustically active and allow clot targeting, they are exciting potential theranostic tools for specific and direct imaging of thrombi, thus enhancing accurate and fast diagnosis of thrombi, as well as intriguing nanocarriers for site-specific delivery of antithrombotic drugs.

4. EXPERIMENTAL SECTION

4.1. Materials. All chemicals and reagents used in this work were used as received with no further processing unless otherwise specified. Analytical reagents used in all experiments: magnesium chloride hexahydrate, $MgCl_2{\cdot}6H_2O$ (Fluka), protease inhibitor cocktail tablets (Roche), glycerol (Astral Scientific), and PFH (FluoroChem). Reagents used for preparation of buffers in isolation of human washed platelets and membrane derivation were purchased from Sigma-Aldrich: sodium citrate, citric acid, D-glucose, theophylline, potassium phosphate dibasic (K_2HPO_4), disodium phosphate (Na_2HPO_4), monosodium phosphate (NaH_2PO_4), sodium chloride (NaCl), sodium bicarbonate ($NaHCO_3$), *N*-2-hydroxyethylpiperazine-*N*-2-ethanesulfonic acid (HEPES), potassium chloride (KCl), calcium chloride dihydrate ($CaCl_2{\cdot}2H_2O$), and ethylenediamine tetraacetic acid (EDTA).

4.2. Preparation of Washed Resting Platelets from Whole Blood. All experiments using human donors were approved by the Alfred Health Human Ethics Committee (project number: 627/17). Blood from healthy human donors was withdrawn using a 19G butterfly needle into syringes containing sodium citrate (Sarstedt). Following collection, blood was supplemented with acid citrate dextrose (ACD) (final concentration of 7:1 (v/v)), enoxaparin (20 U mL^{-1}), and apyrase (0.02 U mL^{-1}). Washed platelets were prepared as described previously.[49] Briefly, PRP was obtained by centrifugation (200*g*, 15 min). PRP was further centrifuged (1400*g*, 10 min), the supernatant removed, and platelets resuspended in platelet wash buffer (4.3 mM K_2HPO_4, 4.3 mM Na_2HPO_4, 24.3 mM NaH_2PO_4, 113 mM NaCl, 5.5 mM D-glucose, and 10 mM theophylline (pH 6.5) containing enoxaparin (20 U mL^{-1}), apyrase (0.02 U mL^{-1}), and bovine serum albumin (0.5%)). A platelet count was obtained using an automated hematological cell counter (Sysmex XN-550, Sysmex). Platelets were pelleted by centrifugation (1200*g*, 10 min) and resuspended in Tyrode's buffer (12 mM $NaHCO_3$, 10 mM HEPES, 137 mM NaCl, 2.7 mM KCl, 5.5 mM D-glucose, 1.8 mM $CaCl_2$, and 1 mM $MgCl_2$) containing apyrase (0.01 U mL^{-1}) to the desired final concentration.

4.3. Preparation of Platelet Membranes from Washed Resting Platelets. Derivation of platelet membranes from washed resting platelets was based on the previously reported method of Hu et al. (2015).[50] Prior to derivation, resting washed platelets were first quantified using an automated cell counter (Sysmex XN-550, Sysmex). The dispersion containing 1.6×10^8 platelets was pelleted in 1.5 mL tubes by centrifugation at 4000*g* for 3 min, followed by redispersion in fresh 1.5 mL 1× PBS with 1 mM EDTA and protease

https://doi.org/10.1021/acsami.4c12024
ACS Appl. Mater. Interfaces 2024, 16, 55142−55154

inhibitor cocktail tablets. Platelet membranes were obtained by repeated freezing at −80 °C for 30 min and thawing at room temperature for 30 min (total of three freeze−thaw cycles), with pelleting by centrifugation at 4000*g* for 3 min and redispersion in fresh 1.5 mL 1× PBS with 1 mM EDTA and protease inhibitor cocktail tablets between cycles. After the last freeze−thaw cycle, the pellets were then redispersed in 200 μL 1× PBS (platelet membrane dispersion).

4.4. Fabrication of Platelet Bubbles. The ultrasound-assisted bubble fabrication procedure employed was based on the work of Vidallon et al. (2021).[14] Briefly, platelet membrane dispersion (200 μL) was combined in a 5 mL glass vial with 500 mg glycerol via vortex mixing, followed by cooling in an ice bath for 10 to 20 min. The glass container containing the platelet−glycerol mixture was sealed with a silicone cap, followed by injection of 20 mL PFC gas−air mixture into the headspace. The cap was punctured to insert a probe sonicator tip, which was positioned a few millimeters below the gas−liquid interface. The mixture was sonicated for 10 s with an acoustic power of 1 W. The glass vial was cooled in an ice bath immediately after sonication for at least 10 min. The concentrated platelet bubble mixture was either used immediately with PBS as the diluent or refrigerated for stability studies prior to dilution to the desired volume concentration using PBS. The theoretical PFH content of PMBs is available in the Supporting Calculations and Table S1 in the Supporting Information. "Bubble-less" control was fabricated by sonicating the platelet−glycerol mixture at the half-volume level, instead of sonication at the gas−liquid interface.

4.5. Size and Surface Charge Measurements. The diluted PMB dispersion was diluted further by 100-fold prior to size and ζ-potential measurement using DLS and electrophoretic light scattering (ELS), respectively, using a Malvern Zetasizer (Malvern Panalytical Ltd.). Bubbles were also observed visually via optical microscopy.

4.6. Morphological Analysis. PMBs were imaged by TEM following previous sample preparation methods for dynamic and unstable colloidal materials.[51] Diluted PMB dispersion (10 μL, 8.0 × 10^8 bubbles) was pipetted onto a Parafilm-covered glass plate. Carbon-coated 300 mesh copper grids were incubated for 5 min on top of the emulsion droplets with the carbon face down. Following incubation, the excess sample was blotted away with filter paper and the grids were placed face down onto 10 μL droplets of 1% aqueous uranyl acetate. The grids were incubated on uranyl acetate for 30 s, after which the uranyl acetate was blotted away with filter paper and the grids allowed to dry. Negatively stained emulsion droplets on the TEM grids were imaged in a JEOL JEM-1400 Plus transmission electron microscope (JEOL USA, Inc.) with an accelerating voltage of 80 keV and at spot size number 2. Digital images were captured with a resolution of 2048 × 2048 pixels.

4.7. Confocal Microscopy. PMB morphology and receptor expression were assessed using confocal microscopy. PMB or human washed platelets were seeded into microscopy chambers with glass coverslip bases (Sarsedt) and allowed to settle for 1 h. PMBs or washed platelets were stained with an anti-CD41 ($GP_{IIb;}$ HIP8, Biolegend), anti-CD42b (GPIb, SZ2, BD), or anti-GPVI (HY101, BD) antibody for 30 min and imaged using confocal microscopy (Nikon A1r).

4.8. Flow Cytometry. Flow cytometry was used to assess the expression of platelet receptors on PMBs, PLT M, and human washed platelets. Populations were determined by forward scatter (FSC) and side scatter (SSC) to differentiate them from human washed platelets. PMBs or human washed platelets were incubated with antibodies against CD41 (GP_{IIb}; HIP8, Biolegend), CD42 (GPIb, SZ2, BD), CD61 (RUU-PL7F12, BD), GPVI (HY101, BD), or relevant isotype controls (fluorescently labeled mouse IgG BD) for 30 min. For activation experiments, PMBs or human washed plateletes were incubated with antibodies against CD62P (P-selectin, BD), or the active conformation of GPIIb/IIIa (PAC-1, BD) for 15 min before being stimulated with thrombin (1 U mL^{-1}) for 30 min. Samples were analyzed using a LSRFortessa X-20 flow cytometer and FlowJo software (BD).

4.9. Platelet Aggregation. The effects of PMBs on platelet aggregation were assessed using LTA. Human PRP was prepared as described in Section 4.2 (without the addition of ACD or enoxaparin) and maintained at 37 °C. PRP was transferred to glass cuvettes and PMBs, platelet membranes or vehicle were added and the change in optical density was measured under stirring conditions (600 rpm). After 5 min the PRP was stimulated with TRAP (30 μM) and aggregation was measured in real time as a decrease in optical density as platelets aggregated and were pulled out of suspension. As the PMBs had different optical properties to the vehicle and platelet membranes, a correction factor was applied by taking the average optical density after addition of PMBs and subtracting this difference. To show that this increased optical density was due to the turbidity of the PMB dispersion, this experiment was also performed in the absence of platelets using PPP.

4.10. Hemocompatibility. The hemocompatibility of the PMBs was assessed as the release of hemoglobin through the absorbance and effect on blood cells using an automated cell counter (Sysmex XN-550, Sysmex). Fresh citrated human whole blood was collected within 1 h of experimentation. Increasing concentrations of PMBs (final concentration range of 0.1−16 × 10^9 PMBs mL^{-1}), PBS, vehicle (PBS−glycerol), or Triton X-100 were added to human whole blood at a ratio of 1:20 (sample/blood) and placed on a roller at 37 °C for 1 h. A 20 μL aliquot of whole blood was taken for analysis using an automated cell counter (Sysmex). Samples were then centrifuged (2000 rpm, 10 min) to separate plasma from blood. Plasma was collected and absorbance at 550 nm was measured using a plate reader.[52] Hemolysis was calculated and normalized to 100% hemolysis (Triton X-100).

4.11. MTT Assay. Viability of human fibroblasts after exposure to PMBs was evaluated using a standard MTT protocol.[53] Briefly, cells (10^4 cells per well) were seeded into 96-well plates in 100 μL volume with cell culture medium (DMEM supplemented with 10% (v/v) FBS, 1% (v/v) penicillin−streptomycin solution and 1% (v/v) L-glutamine) and incubated for 24 h, prior to treatment. Medium from each well was replaced with fresh medium containing different concentrations of PMBs (final concentration range of 0.1−16 × 10^9 PMBs mL^{-1}), followed by incubation at 37 °C for 24 h. MTT solution (10 μL, 5 mg mL^{-1}) was then added per well, followed by a 4-h incubation period at 37 °C. After incubation, the medium was removed and replaced with 100 μL dimethyl sulfoxide (DMSO) to each well to dissolve formazan crystals, followed by spectrophotometric reading at 570 nm. Cell viability was calculated and normalized to 100% using the absorbance of wells with PBS-treated cells.

4.12. Platelet Microbubble Adhesion to Thrombi. The ability of the PMBs to adhere to preformed thrombi was assessed *in vitro*. Platelet thrombi were formed as described previously.[49] Briefly, glass microslides (0.1 × 1 mm; VitroCom) were coated with type I bovine collagen (250 μg mL^{-1}). Anticoagulated whole blood (enoxaparin 40 U mL^{-1}) was perfused through the slides at a constant shear rate of 1800 s^{-1} for 8 min. Slides were rinsed with Tyrode's buffer containing bovine serum albumin (0.5%) to remove unadhered blood cells and 1 mL of fluorescently labeled ($DiIC_{12}$ 1 μg mL^{-1}) PMBs were perfused over the thrombi. Slides were rinsed with Tyrode's buffer and fixed with paraformaldehyde (1%). Slides were imaged using a Nikon A1r confocal microscope and analyzed using ImageJ by applying a common threshold to create regions of interest around thrombi. The mean fluorescence of the PMBs was calculated within these regions of interest.

4.13. *In Vivo* Intravital Microscopy. All animal experiments performed for *in vivo* intravital microscopy were approved by the Alfred Medical Research and Education Precinct Animal Ethics Committee (approval E/8196/2021/B). PMB adherence to preformed thrombi was assessed *in vivo* using a laser-induced mesenteric thrombosis model. Mice were anesthetized using a combination of ketamine (80 mg kg^{-1}) and xylazine (20 mg kg^{-1}). A laparotomy was performed, the mesentery was externalized on a glass stage plate, and a glass coverslip (22 mm × 22 mm, 0.13−0.16 mm thick) was placed over the chosen mesenteric vessels. Prior to imaging, a fluorescent platelet antibody (GPIb DyLight-649, 0.1 μg g^{-1}, Emfret) was

https://doi.org/10.1021/acsami.4c12024
ACS Appl. Mater. Interfaces 2024, 16, 55142−55154

administered by intravenous injection. Intravital imaging was performed using a Zeiss LSM 880 upright microscope. Blood vessels were located using a combination of transmitted light and autofluorescence in the 488 nm channel and an endothelial injury was induced using a single pulsed 405 nm laser (Rapp OptoElectronic), then the resulting thrombus was allowed to form and stabilize before a *Z*-stack was acquired. After the thrombus had been imaged, 150 μL of fluorescently labeled ($DiIC_{12}$, 2 $\mu g\ mL^{-1}$) PMBs (12×10^9 PMB) or vehicle (same volume of PBS−glycerol containing 2 $\mu g\ mL^{-1}$ $DiIC_{12}$) were injected intravenously. The thrombus was located, a time-series video was acquired showing platelet microbubbles in solution adhering to the thrombus, and a *Z*-stack was acquired. Following experimentation, animals were humanely killed. Images were analyzed using ImageJ. A region of interest around the thrombus was drawn using the GPIb platelet marker and applied to the PMB fluorescent channel. A common threshold was applied and the total fluorescence of the PMBs in the region of interest was obtained for the entire *Z*-stack.

4.14. Ultrasound Imaging. The ultrasound contrast-enhancing capabilities of the platelet microbubbles were evaluated via ultrasound imaging using a Vevo 2100 high-frequency ultrasound scanner with a 22−55 MHz MS 550D transducer (FUJIFILM VisualSonics, Inc.).

4.14.1. In Vitro Model for Ultrasound Imaging. Ultrasonograms were obtained from tissue-mimicking phantoms made from 1% agarose hydrogels which were loaded with different concentrations of PMBs (4.0×10^8 to 6×10^9 bubbles). Platelet membranes and PBS were used as controls with three independent experiments ($n = 3$).

4.14.2. In Vivo Model for Ultrasound Imaging. All animal experiments involving ultrasound imaging were approved by the Alfred Medical Research and Education Precinct Animal Ethics Committee (approval E/8335/2022/B). C57BL/6 mice were injected with a combination of ketamine (100 mg kg^{-1}) and xylazine (5 mg kg^{-1}) intraperitoneally. Then, a 1 cm incision was made between the abdomen and thigh of the mouse. A catheter was inserted intravenously into the exposed femoral vein and secured. The mouse was then placed onto a VisualSonics imaging station (VisualSonics Inc., Canada) in a supine position. Ultrasound was performed using the Vevo 2100 system and the 22−55 MHz MS 550D transducer (VisualSonics Inc., Canada). Ultrasound imaging of the inferior vena cava using B-mode and contrast mode ($n = 3$ with multiple frames for each animal) were captured. PBS (control) or PMBs (100 μL containing either 6×10^9 and 12×10^9 bubbles in PBS) were administered via the catheter. Gray values of the ultrasonograms obtained were obtained using ImageJ.

■ ASSOCIATED CONTENT

Supporting Information

The Supporting Information is available free of charge at https://pubs.acs.org/doi/10.1021/acsami.4c12024.

Additional experimental results and supporting calculations of theoretical PFH content in PMBs (PDF)

Representative time-lapse video of *in vivo* thrombosis experiments with PMBs (AVI)

Representative time-lapse video of *in vivo* thrombosis experiments with vehicle control (AVI)

■ AUTHOR INFORMATION

Corresponding Authors

Mark Louis P. Vidallon − *Molecular Imaging and Theranostics Laboratory, Baker Heart and Diabetes Institute, Melbourne, VIC 3004, Australia; Baker Department of Cardiometabolic Health, University of Melbourne, Parkville, VIC 3010, Australia; School of Chemistry, Monash University, Clayton, VIC 3800, Australia; Baker Department of Cardiovascular Research, Translation and Implementation, La Trobe University, Bundoora, VIC 3086, Australia;* orcid.org/0000-0002-0026-3906; Email: marklouis.vidallon@unimelb.edu.au

Xiaowei Wang − *Molecular Imaging and Theranostics Laboratory, Baker Heart and Diabetes Institute, Melbourne, VIC 3004, Australia; Baker Department of Cardiometabolic Health, University of Melbourne, Parkville, VIC 3010, Australia; Baker Department of Cardiovascular Research, Translation and Implementation, La Trobe University, Bundoora, VIC 3086, Australia; School of Translational Medicine, Monash University, Melbourne, VIC 3004, Australia;* orcid.org/0000-0001-8658-7399; Email: xiaoweiw@unimelb.edu.au

Authors

Mitchell J. Moon − *Baker Department of Cardiometabolic Health, University of Melbourne, Parkville, VIC 3010, Australia; Atherothrombosis and Vascular Biology Laboratory, Baker Heart and Diabetes Institute, Melbourne, VIC 3004, Australia;* orcid.org/0000-0001-9345-5001

Haikun Liu − *Molecular Imaging and Theranostics Laboratory, Baker Heart and Diabetes Institute, Melbourne, VIC 3004, Australia; Baker Department of Cardiometabolic Health, University of Melbourne, Parkville, VIC 3010, Australia*

Yuyang Song − *Molecular Imaging and Theranostics Laboratory, Baker Heart and Diabetes Institute, Melbourne, VIC 3004, Australia; Baker Department of Cardiometabolic Health, University of Melbourne, Parkville, VIC 3010, Australia*

Simon Crawford − *Ramaciotti Centre for Cryo-electron Microscopy, Monash University, Clayton, VIC 3800, Australia*

Boon Mian Teo − *School of Chemistry, Monash University, Clayton, VIC 3800, Australia;* orcid.org/0000-0002-9188-5451

James D. McFadyen − *Baker Department of Cardiometabolic Health, University of Melbourne, Parkville, VIC 3010, Australia; Atherothrombosis and Vascular Biology Laboratory, Baker Heart and Diabetes Institute, Melbourne, VIC 3004, Australia; Department of Clinical Hematology, The Alfred Hospital, Melbourne, VIC 3004, Australia; School of Translational Medicine, Monash University, Melbourne, VIC 3004, Australia*

Alexis I. Bishop − *School of Physics and Astronomy, Monash University, Clayton, VIC 3800, Australia*

Rico F. Tabor − *School of Chemistry, Monash University, Clayton, VIC 3800, Australia;* orcid.org/0000-0003-2926-0095

Karlheinz Peter − *Baker Department of Cardiometabolic Health, University of Melbourne, Parkville, VIC 3010, Australia; Baker Department of Cardiovascular Research, Translation and Implementation, La Trobe University, Bundoora, VIC 3086, Australia; Atherothrombosis and Vascular Biology Laboratory, Baker Heart and Diabetes Institute, Melbourne, VIC 3004, Australia; School of Translational Medicine, Monash University, Melbourne, VIC 3004, Australia*

Complete contact information is available at: https://pubs.acs.org/10.1021/acsami.4c12024

Author Contributions

[¶]M.L.P.V. and M.J.M. contributed equally as the first authors to this work. K.P. and X.W. contributed equally as the senior authors to this work.

Notes

The authors declare no competing financial interest.

■ ACKNOWLEDGMENTS

The authors would like to thank the Baker Heart and Diabetes Institute Microscopy Platform for technical and equipment support and AMREP animal services for animal husbandry. The authors acknowledge the use of instruments and assistance from the Monash Ramaciotti Centre for Cryo-Electron Microscopy, a Node of Microscopy Australia. M.L.P.V. is supported by National Heart Foundation of Australia Postdoctoral Fellowship; Y.S. is supported by a University of Melbourne Scholarship; H.L. is supported by the University of Melbourne through a Baker Department of Cardiometabolic Health PhD Scholarship; K.P. is supported by an NHMRC L3 Investigator Fellowship; X.W. is supported by National Heart Foundation of Australia Future Leader and Baker Fellowships. M.L.P.V., M.J.M., K.P., and X.W. designed the study. M.L.P.V., B.T., A.I.B., and R.F.T. designed and optimized the PMB formulation. M.L.P.V., M.J.M., Y.S., H.L., S.C., J.D.M., and X.W. were involved in the methodology and data acquisition. K.P. and X.W. funded the research. M.L.P.V., M.J.M., H.L., Y.S., and X.W. analyzed the data. M.L.P.V., M.J.M., and X.W. drafted the manuscript. M.L.P.V., M.J.M., H.L., Y.S., A.I.B., R.F.T., K.P., and X.W. provided critical review of the content of the manuscript. All authors approved the final version of the manuscript before submission.

■ REFERENCES

(1) Wang, X.; Palasubramaniam, J.; Gkanatsas, Y.; Hohmann, J. D.; Westein, E.; Kanojia, R.; Alt, K.; Huang, D.; Jia, F.; Ahrens, I.; Medcalf, R. L.; Peter, K.; Hagemeyer, C. E. Towards Effective and Safe Thrombolysis and Thromboprophylaxis. *Circ. Res.* **2014**, *114* (7), 1083−1093.

(2) Bates, S. M.; Jaeschke, R.; Stevens, S. M.; Goodacre, S.; Wells, P. S.; Stevenson, M. D.; Kearon, C.; Schunemann, H. J.; Crowther, M.; Pauker, S. G.; Makdissi, R.; Guyatt, G. H. Diagnosis of DVT: Antithrombotic Therapy and Prevention of Thrombosis, 9th ed: American College of Chest Physicians Evidence-Based Clinical Practice Guidelines. *Chest* **2012**, *141* (2 Suppl), e351S−e418S.

(3) Tovey, C.; Wyatt, S. Diagnosis, investigation, and management of deep vein thrombosis. *BMJ* **2003**, *326* (7400), 1180−1184.

(4) Wang, X.; Ziegler, M.; McFadyen, J. D.; Peter, K. Molecular imaging of arterial and venous thrombosis. *Br. J. Pharmacol.* **2021**, *178* (21), 4246−4269.

(5) Liu, H.; Pietersz, G.; Peter, K.; Wang, X. Nanobiotechnology approaches for cardiovascular diseases: site-specific targeting of drugs and nanoparticles for atherothrombosis. *J. Nanobiotechnol.* **2022**, *20* (1), No. 75.

(6) Heestermans, M.; Poenou, G.; Hamzeh-Cognasse, H.; Cognasse, F.; Bertoletti, L. Anticoagulants: A Short History, Their Mechanism of Action, Pharmacology, and Indications. *Cells* **2022**, *11* (20), 3214.

(7) Wang, X.; Gkanatsas, Y.; Palasubramaniam, J.; Hohmann, J. D.; Chen, Y. C.; Lim, B.; Hagemeyer, C. E.; Peter, K. Thrombus-Targeted Theranostic Microbubbles: A New Technology towards Concurrent Rapid Ultrasound Diagnosis and Bleeding-free Fibrinolytic Treatment of Thrombosis. *Theranostics* **2016**, *6* (5), 726−738.

(8) Vidallon, M. L. P.; Teo, B. M.; Bishop, A. I.; Tabor, R. F. Next-Generation Colloidal Materials for Ultrasound Imaging Applications. *Ultrasound Med. Biol.* **2022**, *48* (8), 1373−1396.

(9) Najaflou, M.; Shahgolzari, M.; Khosroushahi, A. Y.; Fiering, S. Tumor-Derived Extracellular Vesicles in Cancer Immunoediting and Their Potential as Oncoimmunotherapeutics. *Cancers* **2023**, *15* (1), 82.

(10) Chen, C.; Song, M.; Du, Y.; Yu, Y.; Li, C.; Han, Y.; Yan, F.; Shi, Z.; Feng, S. Tumor-Associated-Macrophage-Membrane-Coated Nanoparticles for Improved Photodynamic Immunotherapy. *Nano Lett.* **2021**, *21* (13), 5522−5531.

(11) Liu, C.; Wang, D.; Zhang, S.; Cheng, Y.; Yang, F.; Xing, Y.; Xu, T.; Dong, H.; Zhang, X. Biodegradable Biomimic Copper/Manganese Silicate Nanospheres for Chemodynamic/Photodynamic Synergistic Therapy with Simultaneous Glutathione Depletion and Hypoxia Relief. *ACS Nano* **2019**, *13* (4), 4267−4277.

(12) Kroll, A. V.; Fang, R. H.; Zhang, L. Biointerfacing and Applications of Cell Membrane-Coated Nanoparticles. *Bioconjugate Chem.* **2017**, *28* (1), 23−32.

(13) Wang, D.; Wang, S.; Zhou, Z.; Bai, D.; Zhang, Q.; Ai, X.; Gao, W.; Zhang, L. White Blood Cell Membrane-Coated Nanoparticles: Recent Development and Medical Applications. *Adv. Healthcare Mater.* **2022**, *11* (7), No. 2101349.

(14) Vidallon, M. L. P.; Tabor, R. F.; Bishop, A. I.; Teo, B. M. Ultrasound-assisted fabrication of acoustically active, erythrocyte membrane "bubbles". *Ultrason. Sonochem.* **2021**, *72*, No. 105429.

(15) Wei, X.; Ying, M.; Dehaini, D.; Su, Y.; Kroll, A. V.; Zhou, J.; Gao, W.; Fang, R. H.; Chien, S.; Zhang, L. Nanoparticle Functionalization with Platelet Membrane Enables Multifactored Biological Targeting and Detection of Atherosclerosis. *ACS Nano* **2018**, *12* (1), 109−116.

(16) Litvinov, R. I.; Farrell, D. H.; Weisel, J. W.; Bennett, J. S. The Platelet Integrin αIIbβ3 Differentially Interacts with Fibrin Versus Fibrinogen. *J. Biol. Chem.* **2016**, *291* (15), 7858−7867.

(17) Canobbio, I.; Balduini, C.; Torti, M. Signalling through the platelet glycoprotein Ib-V-IX complex. *Cell. Signalling* **2004**, *16* (12), 1329−1344.

(18) Nieswandt, B.; Watson, S. P. Platelet-collagen interaction: is GPVI the central receptor? *Blood* **2003**, *102* (2), 449−461.

(19) Li, M.; Wang, L.; Tang, D.; Zhao, G.; Ni, Z.; Gu, N.; Yang, F. Hemodynamic Mimic Shear Stress for Platelet Membrane Nanobubbles Preparation and Integrin αIIbβ3 Conformation Regulation. *Nano Lett.* **2022**, *22* (1), 271−279.

(20) Lafond, M.; Watanabe, A.; Yoshizawa, S.; Umemura, S.-i.; Tachibana, K. Cavitation-threshold Determination and Rheological-parameters Estimation of Albumin-stabilized Nanobubbles. *Sci. Rep.* **2018**, *8* (1), No. 7472.

(21) Agarwal, A.; Ng, W. J.; Liu, Y. Principle and applications of microbubble and nanobubble technology for water treatment. *Chemosphere* **2011**, *84* (9), 1175−1180.

(22) Exner, A. A.; Kolios, M. C. Bursting microbubbles: How nanobubble contrast agents can enable the future of medical ultrasound molecular imaging and image-guided therapy. *Curr. Opin. Colloid Interface Sci.* **2021**, *54*, No. 101463.

(23) Myers, J. Z.; Navarro-Becerra, J. A.; Borden, M. A. Nanobubbles are Non-Echogenic for Fundamental-Mode Contrast-Enhanced Ultrasound Imaging. *Bioconjugate Chem.* **2022**, *33* (6), 1106−1113.

(24) Wang, X.; Hagemeyer, C. E.; Hohmann, J. D.; Leitner, E.; Armstrong, P. C.; Jia, F.; Olschewski, M.; Needles, A.; Peter, K.; Ahrens, I. Novel Single-Chain Antibody-Targeted Microbubbles for Molecular Ultrasound Imaging of Thrombosis. *Circulation* **2012**, *125* (25), 3117−3126.

(25) Wang, X.; Peter, K. Molecular Imaging of Atherothrombotic Diseases. *Arterioscler., Thromb., Vasc. Biol.* **2017**, *37* (6), 1029−1040.

(26) Walsh, A. P. G.; Gordon, H. N.; Peter, K.; Wang, X. Ultrasonic particles: An approach for targeted gene delivery. *Adv. Drug Delivery Rev.* **2021**, *179*, No. 113998.

(27) Hu, X.; Zhao, P.; Zhang, J.; Zhu, Y.; Zhou, W.; Hong, K.; Sun, R.; Wang, Y.; Lu, Y.; Liu, Y. Ultrasound-assisted biomimetic nanobubbles for targeted treatment of atherosclerosis. *Nanomed. Nanotechnol. Biol. Med.* **2023**, *51*, No. 102682.

https://doi.org/10.1021/acsami.4c12024
ACS Appl. Mater. Interfaces 2024, 16, 55142−55154

(28) Yang, J.; Miao, X.; Guan, Y.; Chen, C.; Chen, S.; Zhang, X.; Xiao, X.; Zhang, Z.; Xia, Z.; Yin, T.; Hei, Z.; Yao, W. Microbubble Functionalization with Platelet Membrane Enables Targeting and Early Detection of Sepsis-Induced Acute Kidney Injury. *Adv. Healthcare Mater.* **2021**, *10* (23), No. 2101628.
(29) Li, M.; Liu, Y.; Chen, J.; Liu, T.; Gu, Z.; Zhang, J.; Gu, X.; Teng, G.; Yang, F.; Gu, N. Platelet bio-nanobubbles as microvascular recanalization nanoformulation for acute ischemic stroke lesion theranostics. *Theranostics* **2018**, *8* (18), 4870−4883.
(30) Monash University. Compositions and methods of use Australian Patent No., AU2019903896, 2019, IP Australia.
(31) Ibsen, S.; Benchimol, M.; Simberg, D.; Schutt, C.; Steiner, J.; Esener, S. A novel nested liposome drug delivery vehicle capable of ultrasound triggered release of its payload. *J. Controlled Release* **2011**, *155* (3), 358−366.
(32) Lentacker, I.; De Geest, B. G.; Vandenbroucke, R. E.; Peeters, L.; Demeester, J.; De Smedt, S. C.; Sanders, N. N. Ultrasound-Responsive Polymer-Coated Microbubbles That Bind and Protect DNA. *Langmuir* **2006**, *22* (17), 7273−7278.
(33) Nicolson, G. L. The Fluid—Mosaic Model of Membrane Structure: Still relevant to understanding the structure, function and dynamics of biological membranes after more than 40years. *Biochim. Biophys. Acta, Biomembr.* **2014**, *1838* (6), 1451−1466.
(34) Abou-Saleh, R. H.; Peyman, S. A.; Johnson, B. R. G.; Marston, G.; Ingram, N.; Bushby, R.; Coletta, P. L.; Markham, A. F.; Evans, S. D. The influence of intercalating perfluorohexane into lipid shells on nano and microbubble stability. *Soft Matter* **2016**, *12* (34), 7223−7230.
(35) Montague, S. J.; Andrews, R. K.; Gardiner, E. E. Mechanisms of receptor shedding in platelets. *Blood* **2018**, *132* (24), 2535−2545.
(36) Waters, L.; Padula, M. P.; Marks, D. C.; Johnson, L. Calcium chelation: a novel approach to reduce cryopreservation-induced damage to frozen platelets. *Transfusion* **2020**, *60* (7), 1552−1563.
(37) Waters, L.; Padula, M. P.; Marks, D. C.; Johnson, L. Cryopreserved platelets demonstrate reduced activation responses and impaired signaling after agonist stimulation. *Transfusion* **2017**, *57* (12), 2845−2857.
(38) Miles, J.; Bailey, S. L.; Obenaus, A. M.; Mollica, M. Y.; Usaneerungrueng, C.; Byrne, D.; Fang, L.; Flynn, J. R.; Corson, J.; Osborne, B.; Houck, K.; Wang, Y.; Shen, Y.; Fu, X.; Dong, J.-F.; Sniadecki, N. J.; Stolla, M. Storage temperature determines platelet GPVI levels and function in mice and humans. *Blood Adv.* **2021**, *5* (19), 3839−3849.
(39) Khan, F.; Singh, K.; Friedman, M. T. Artificial Blood: The History and Current Perspectives of Blood Substitutes. *Discoveries* **2020**, *8* (1), No. e104.
(40) Kakaei, N.; Amirian, R.; Azadi, M.; Mohammadi, G.; Izadi, Z. Perfluorocarbons: A perspective of theranostic applications and challenges. *Front. Bioeng. Biotechnol.* **2023**, *11*, No. 1115254.
(41) Yap, M. L.; McFadyen, J. D.; Wang, X.; Zia, N. A.; Hohmann, J. D.; Ziegler, M.; Yao, Y.; Pham, A.; Harris, M.; Donnelly, P. S.; Hogarth, P. M.; Pietersz, G. A.; Lim, B.; Peter, K. Targeting Activated Platelets: A Unique and Potentially Universal Approach for Cancer Imaging. *Theranostics* **2017**, *7* (10), 2565−2574.
(42) Savage, B.; Ruggeri, Z. M. Selective recognition of adhesive sites in surface-bound fibrinogen by glycoprotein IIb-IIIa on nonactivated platelets. *J. Biol. Chem.* **1991**, *266* (17), 11227−11233.
(43) Zhao, Y.; Xie, R.; Yodsanit, N.; Ye, M.; Wang, Y.; Wang, B.; Guo, L. W.; Kent, K. C.; Gong, S. Hydrogen peroxide-responsive platelet membrane-coated nanoparticles for thrombus therapy. *Biomater Sci.* **2021**, *9* (7), 2696−2708.
(44) Refaat, A.; del Rosal, B.; Bongcaron, V.; Walsh, A. P. G.; Pietersz, G.; Peter, K.; Moulton, S. E.; Wang, X. Activated Platelet-Targeted IR780 Immunoliposomes for Photothermal Thrombolysis. *Adv. Funct. Mater.* **2023**, *33* (4), No. 2209019.
(45) Papa, A.-L.; Jiang, A.; Korin, N.; Chen, M. B.; Langan, E. T.; Waterhouse, A.; Nash, E.; Caroff, J.; Graveline, A.; Vernet, A.; Mammoto, A.; Mammoto, T.; Jain, A.; Kamm, R. D.; Gounis, M. J.; Ingber, D. E. Platelet decoys inhibit thrombosis and prevent metastatic tumor formation in preclinical models. *Sci. Transl. Med.* **2019**, *11* (479), No. eaau5898.
(46) Kaneti, L.; Bronshtein, T.; Malkah Dayan, N.; Kovregina, I.; Letko Khait, N.; Lupu-Haber, Y.; Fliman, M.; Schoen, B. W.; Kaneti, G.; Machluf, M. Nanoghosts as a Novel Natural Nonviral Gene Delivery Platform Safely Targeting Multiple Cancers. *Nano Lett.* **2016**, *16* (3), 1574−1582.
(47) Korin, N.; Kanapathipillai, M.; Matthews, B. D.; Crescente, M.; Brill, A.; Mammoto, T.; Ghosh, K.; Jurek, S.; Bencherif, S. A.; Bhatta, D.; Coskun, A. U.; Feldman, C. L.; Wagner, D. D.; Ingber, D. E. Shear-Activated Nanotherapeutics for Drug Targeting to Obstructed Blood Vessels. *Science* **2012**, *337* (6095), 738−742.
(48) Li, Q.; Liu, X.; Chang, M.; Lu, Z. Thrombolysis Enhancing by Magnetic Manipulation of Fe_3O_4 Nanoparticles. *Materials* **2018**, *11* (11), 2313.
(49) Selvadurai, M. V.; Moon, M. J.; Mountford, S. J.; Ma, X.; Zheng, Z.; Jennings, I. G.; Setiabakti, N. M.; Iman, R. P.; Brazilek, R. J.; Z Abidin, N. A.; Chicanne, G.; Severin, S.; Nicholls, A. J.; Wong, C. H. Y.; Rinckel, J.-Y.; Eckly, A.; Gachet, C.; Nesbitt, W. S.; Thompson, P. E.; Hamilton, J. R. Disrupting the platelet internal membrane via PI3KC2α inhibition impairs thrombosis independently of canonical platelet activation. *Sci. Transl. Med.* **2020**, *12* (553), No. eaar8430.
(50) Hu, C. M.; Fang, R. H.; Wang, K. C.; Luk, B. T.; Thamphiwatana, S.; Dehaini, D.; Nguyen, P.; Angsantikul, P.; Wen, C. H.; Kroll, A. V.; Carpenter, C.; Ramesh, M.; Qu, V.; Patel, S. H.; Zhu, J.; Shi, W.; Hofman, F. M.; Chen, T. C.; Gao, W.; Zhang, K.; Chien, S.; Zhang, L. Nanoparticle biointerfacing by platelet membrane cloaking. *Nature* **2015**, *526* (7571), 118−121.
(51) Vidallon, M. L. P.; Giles, L. W.; Pottage, M. J.; Butler, C. S. G.; Crawford, S. A.; Bishop, A. I.; Tabor, R. F.; de Campo, L.; Teo, B. M. Tracking the heat-triggered phase change of polydopamine-shelled, perfluorocarbon emulsion droplets into microbubbles using neutron scattering. *J. Colloid Interface Sci.* **2022**, *607*, 836−847.
(52) Refaat, A.; del Rosal, B.; Palasubramaniam, J.; Pietersz, G.; Wang, X.; Moulton, S. E.; Peter, K. Near-infrared light-responsive liposomes for protein delivery: Towards bleeding-free photo-thermally-assisted thrombolysis. *J. Controlled Release* **2021**, *337*, 212−223.
(53) Riss, T. L.; Moravec, R. A.; Niles, A. L.; Duellman, S.; Benink, H. A.; Worzella, T. J.; Minor, L. Cell Viability Assays. In *The Assay Guidance Manual*; Markossian, S.; Grossman, A.; Brimacombe, K.; Arkin, M.; Auld, D.; Austin, C.; Baell, J.; Chung, T. D. Y.; Coussens, N. P.; Dahlin, J. L.; Devanarayan, V.; Foley, T. L.; Glicksman, M.; Gorshkov, K.; Haas, J. V.; Hall, M. D.; Hoare, S.; Inglese, J.; Iversen, P. W.; Kales, S. C.; Lal-Nag, M.; Li, Z.; McGee, J.; McManus, O.; Riss, T.; Saradjian, P.; Sittampalam, G. S.; Tarselli, M.; Trask, O. J., Jr.; Wang, Y.; Weidner, J. R.; Wildey, M. J.; Wilson, K.; Xia, M.; Xu, X., Eds.; Eli Lilly & Company and the National Center for Advancing Translational Sciences, 2013 (Updated 2016).

https://doi.org/10.1021/acsami.4c12024
ACS Appl. Mater. Interfaces 2024, 16, 55142−55154